Proceedings of the 2006 IASME/WSEAS International Conference on Continuum Mechanics, Chalkida, Greece, May 11-13, 2006 (pp79-84)

Numerical simulations of second–grade fluids in curved pipes

NADIR ARADA
Fac. de Ciências e Tecnologia–UNL
Dep. de Matemática and CMA
Quinta da Torre, 2829-516 Caparica
PORTUGAL

PAULO CORREIA
Universidade de Évora
Dep. de Matemática and CIMA–UE
R. Romão Ramalho 59, 7000 Évora
PORTUGAL

ADÉLIA SEQUEIRA
Instituto Superior Técnico
Dep. de Matemática and CEMAT
Av. Rovisco Pais 1, 1049 Lisboa
PORTUGAL

Abstract: This paper is concerned with a numerical study of steady fully developed second-grade flows in a curved pipe of circular cross-section and arbitrary curvature ratio, driven by a pressure drop. The qualitative behaviour of the secondary flows is analyzed with respect to inertia and viscoelasticity effects.

Key–Words: Second–grade fluids, finite elements, curved pipes, secondary flows.

1 Introduction

Fully developed viscous flow in a curved pipe with circular cross-section was first studied theoretically by Dean ([7], [8]) applying regular perturbation methods. He showed that for small curvature ratio the flow depends only on a single parameter, the so-called *Dean number*. In [12], Soh and Berger solved the Navier-Stokes equations for the fully developed flow of an homogeneous Newtonian fluid in a curved pipe of circular cross-section for arbitrary curvature ratio. They solved numerically the Navier-Stokes system in the primitive variables form using a finite difference scheme. Closed form perturbation solutions for a second order model were obtained by several authors in the special case where the second normal stress coefficient is zero.

For this model, Jitchote and Robertson [10] obtained analytical solutions to the perturbation equations and analyze the effects of non-zero second normal stress coefficient on the behaviour of the solution. Theoretical results regarding this problem using a splitting method were obtained by Coscia and Robertson [6].

Our aim here is to apply the finite element method to the second-grade model for fully developped flows in a curved pipe and analyze the non-Newtonian effects of the flow. Quantitative and qualitative behaviour of the axial velocity and the stream function of creeping and inertial second-grade fluids are also studied. Similar and other techniques have been applied to different non-Newtonian models (see [2], [3], [9], [11]).

2 Governing equations

We consider steady isothermal flows of incompressible second-grade fluids in a curved pipe $\Omega \subset \mathbb{R}^3$ with boundary $\partial\Omega$, constant circular cross–section Ω_S of radius r with the line of centers coiled in a circle of radius R (see Figure 1).

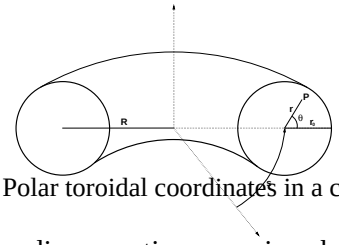

Figure 1: Polar toroidal coordinates in a curved pipe.

The corresponding equations are given by

$$\begin{cases} -\mu\Delta\mathbf{u} - \widetilde{\alpha}_1\mathbf{u}\cdot\nabla\Delta\mathbf{u} + \rho\mathbf{u}\cdot\nabla\mathbf{u} + \nabla\pi = \nabla\cdot\widetilde{\mathbf{L}}(\mathbf{u}) \\ \nabla\cdot\mathbf{u} = 0, \text{ in } \Omega \\ \mathbf{u} = 0, \text{ on } \partial\Omega \end{cases}$$

where $\mathbf{u}$ is the fluid velocity, π is the pressure, μ is the viscosity, ρ is the constant density, $\widetilde{\alpha}_1$ and $\widetilde{\alpha}_2$ are the Rivlin-Ericksen material constants, and $\widetilde{\mathbf{L}}(\mathbf{u})$ is a nonlinear term given by

$$\widetilde{\mathbf{L}}(\mathbf{u}) = \widetilde{\alpha}_1\nabla\mathbf{u}^T\big(\nabla\mathbf{u}+\nabla\mathbf{u}^T\big) + (\widetilde{\alpha}_1+\widetilde{\alpha}_2)\big(\nabla\mathbf{u}+\nabla\mathbf{u}^T\big)^2.$$

We consider an adimensionalised formulation of the previous system by introducing the following quantities

$$\mathbf{x} = \frac{\widetilde{\mathbf{x}}}{a}, \qquad \mathbf{u} = \frac{\widetilde{\mathbf{u}}}{U}, \qquad \pi = \frac{\widetilde{\pi} a}{\mu U},$$

where the symbol $\widetilde{\ }$ is attached to dimensional parameters (U represents a characteristic velocity of the flow). We also introduce the Reynolds number $\mathcal{R}e$ and two non–dimensional ratios involving the constant material moduli $\widetilde{\alpha}_1$ and $\widetilde{\alpha}_2$,

$$\mathcal{R}e = \tfrac{\rho U a}{\mu}, \qquad \alpha_1 = \tfrac{U\widetilde{\alpha}_1}{\mu a}, \qquad \alpha_2 = \tfrac{U\widetilde{\alpha}_2}{\mu a}.$$

The dimensionless system takes the form

$$\begin{cases} -\Delta\mathbf{u} - \alpha_1 \mathbf{u}\cdot\nabla\Delta\mathbf{u} + \mathcal{R}e\,\mathbf{u}\cdot\nabla\mathbf{u} + \nabla\pi = \nabla\cdot\mathbf{L}(\mathbf{u}) \\ \nabla\cdot\mathbf{u} = 0 \\ \mathbf{u} = 0 \end{cases} \tag{1}$$

with

$$\mathbf{L}(\mathbf{u}) = \alpha_1 \nabla\mathbf{u}^T\big(\nabla\mathbf{u}+\nabla\mathbf{u}^T\big) + (\alpha_1+\alpha_2)\big(\nabla\mathbf{u}+\nabla\mathbf{u}^T\big)^2.$$

System (1) can be rewritten in the following equivalent form involving a Stokes system and a transport equation,

$$\begin{cases} -\Delta\mathbf{u} + \nabla p = \boldsymbol{\sigma} \\ \nabla\cdot\mathbf{u} = 0 \\ \mathbf{u} = 0 \\ \boldsymbol{\sigma} + \alpha_1\mathbf{u}\cdot\nabla\boldsymbol{\sigma} = \nabla\cdot\big(\mathbf{L}(\mathbf{u}) - \mathcal{R}e\,\mathbf{u}\otimes\mathbf{u} - \alpha_1 p\nabla\mathbf{u}^T\big), \end{cases} \tag{2}$$

where the new variable p is given by $\pi = p + \alpha_1\mathbf{u}\cdot\nabla p$. Throughout the paper, we consider the particular case of $\alpha_1 + \alpha_2 = 0$, corresponding to a thermodynamical compatibility condition. For a more detailed analysis of this problem see [5].

3 Formulation in polar toroidal coordinates

Since we are interested in studying the behaviour of steady flows in a curved pipe with circular cross-section, it is more convenient to use the polar toroidal coordinate system, in the variables $(\widetilde{r}, \widetilde{\theta}, \widetilde{s})$, defined with respect to the rectangular cartesian coordinates $(\widetilde{x}, \widetilde{y}, \widetilde{z})$ through the relations

$$\widetilde{x} = (R + \widetilde{r}\cos\theta)\cos\tfrac{\widetilde{s}}{R},$$

$$\widetilde{y} = (R + \widetilde{r}\cos\theta)\sin\tfrac{\widetilde{s}}{R}, \quad \widetilde{z} = \widetilde{r}\sin\theta,$$

with $0 < r_0 < R$, $0 \le \widetilde{\theta} < 2\pi$ and $0 \le \widetilde{s} < \pi R$. Introducing the axial variable and the pipe curvature ratio

$$s = \tfrac{\widetilde{s}}{r_0}, \qquad \delta = \tfrac{r_0}{R},$$

the corresponding non-dimensional coordinate system is given by

$$x = \big(\tfrac{1}{\delta} + r\cos\theta\big)\cos(s\delta),$$

$$y = \big(\tfrac{1}{\delta} + r\cos\theta\big)\sin(s\delta), \qquad z = r\sin\theta,$$

with $\delta < 1$, $0 \le \theta < 2\pi$ and $0 \le s < \frac{\pi}{\delta}$. Let us now formulate problem (2) in this new coordinate system. To simplify the notation we set

$$\beta_1 = r\delta\sin\theta, \qquad \beta_2 \equiv \beta_2(r,\theta) = r\delta\cos\theta,$$

$$\beta \equiv \beta(r,\theta) = 1 + r\delta\cos\theta.$$

Since we consider fully developed flows, the components of the velocity are independent of the variable s, i.e.

$$\tfrac{\partial u}{\partial s} = \tfrac{\partial v}{\partial s} = \tfrac{\partial w}{\partial s} \equiv 0. \tag{3}$$

Consequently the axial component of the pressure gradient is a constant and the stress tensor is also independent of the variable s

$$\tfrac{\partial p}{\partial s} = -p^*, \qquad \tfrac{\partial \boldsymbol{\tau}}{\partial s} = 0. \tag{4}$$

Taking into account (3)-(4) and using standard arguments, we rewrite problem (2) in the toroidal coordinates (r, θ, s). This problem is defined in the (bidimensional) set

$$\Sigma = \big\{(r,\theta) \in \mathbb{R}^2 \mid 0 < r < 1,\ 0 < \theta \le 2\pi\big\},$$

and reads as follows

Find $(\mathbf{u} \equiv (u,v,w), p, \widehat{\sigma} \equiv (r\beta)^2\,\sigma)$ solution of

$$\begin{cases} \mathcal{A}u + \big(\beta^2 + \beta_2^2\big)\,u - \beta_1(\beta+\beta_2)v + 2\beta^2\,\frac{\partial v}{\partial\theta} \\ \qquad\qquad + (r\beta)^2\frac{\partial p}{\partial r} = \widehat{\sigma}_1 \\ \mathcal{A}v + \big(\beta^2 + \beta_1^2\big)\,v + \beta_1(\beta-\beta_2)u - 2\beta^2\,\frac{\partial u}{\partial\theta} \\ \qquad\qquad + r\beta^2\,\frac{\partial p}{\partial\theta} = \widehat{\sigma}_2 \\ \mathcal{A}w + (r\delta)^2 w - r^2\beta\,p^* = \widehat{\sigma}_3 \\ r\beta\,\widehat{\sigma}_i + \alpha_1\big(r\beta u\,\frac{\partial\widehat{\sigma}_i}{\partial r} + \beta v\,\frac{\partial\widehat{\sigma}_i}{\partial\theta}\big) = F_i(\mathbf{u}, p, \widehat{\boldsymbol{\sigma}}) \end{cases} \tag{5}$$

for $i = 1, 2, 3$, with

$$\mathcal{A}\psi = -r\beta\tfrac{\partial}{\partial r}\big(r\beta\tfrac{\partial\psi}{\partial r}\big) - \beta\tfrac{\partial}{\partial\theta}\big(\beta\tfrac{\partial\psi}{\partial\theta}\big)$$

and

$$F_1(\mathbf{u}, p, \widehat{\boldsymbol{\sigma}}) = (r\beta)^3\big(\nabla\cdot(\mathbf{L}(\mathbf{u}) - \alpha_1 p\nabla\mathbf{u}^T)\big)_r$$
$$+\alpha_1\big(2\,(\beta+\beta_2)u\widehat{\sigma}_1 - 2\beta_1 v\widehat{\sigma}_1 + \beta v\widehat{\sigma}_2 + \beta_2 w\widehat{\sigma}_3\big)$$

$$F_2(\mathbf{u}, p, \widehat{\boldsymbol{\sigma}}) = (r\beta)^3\big(\nabla\cdot(\mathbf{L}(\mathbf{u}) - \alpha_1 p\nabla\mathbf{u}^T)\big)_\theta$$
$$+\alpha_1\big(2\,(\beta+\beta_2)u\widehat{\sigma}_2 - 2\beta_1 v\widehat{\sigma}_2 - \beta v\widehat{\sigma}_1 - \beta_1 w\widehat{\sigma}_3\big)$$

$$F_3(\mathbf{u}, p, \widehat{\boldsymbol{\sigma}}) = (r\beta)^3\big(\nabla\cdot(\mathbf{L}(\mathbf{u}) - \alpha_1 p\nabla\mathbf{u}^T)\big)_s$$
$$+\alpha_1\big(2\,(\beta+\beta_2)u\widehat{\sigma}_3 - 2\beta_1 v\widehat{\sigma}_3 + \beta_1 w\widehat{\sigma}_2 - \beta_2 w\widehat{\sigma}_1\big)$$

4 Numerical results

We use finite element methods to obtain approximate solutions to system (5). The numerical algorithm is based on Newton's method, with the non-linear part explicitely calculated at each iteration step. As indicated in Figure 2, a Stokes system is solved for $(\mathbf{u}, p)$, a Poisson equation is solved for the axial velocity w and a transport equation for $\boldsymbol{\sigma}$. The velocity is set to zero on the lateral surface of the pipe.

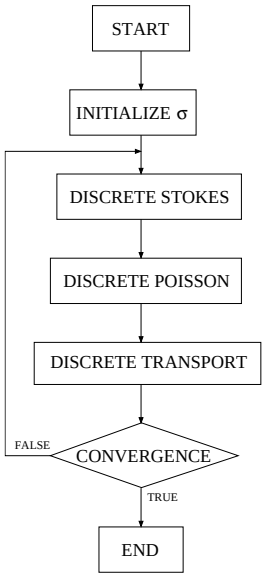

Figure 2: Algorithm.

In order to study the non-Newtonian effects of the flows, we compare the quantitative and qualitative behaviour of the axial velocity and the stream function of both creeping and inertial flows of second-grade fluids. Using a continuation method on the characteristic parameters (the Reynolds number $\mathcal{R}e$ and the viscoelastic parameter α_1), we obtain numerical results in different flow situations.

Introducing an adimensionalised stream function ψ we obtain the following identities for the velocity $\mathbf{u} \equiv (u, v)$,

$$u = -\tfrac{1}{r\beta}\tfrac{\partial \psi}{\partial \theta}\ , \qquad v = \tfrac{1}{\beta}\tfrac{\partial \psi}{\partial r}\ .$$

4.1 Newtonian flows

It is interesting to compare the qualitative behaviour of the flow for second-grade fluids with that of Newtonian fluids. For these purposes, we first consider typical contours of the axial velocity and of the stream function in the case of Newtonian fluids. In the case of creeping fluids ($\mathcal{R}e = 0$), a Poiseuille solution is displayed for a small curvature ratio ($\delta = 0.001$). There is no secondary motion and the contours of the axial velocity w are circles, centered about the central axis (see Figure 3_a). In contrast, as can be seen in Figure 3_b, the contours are shifted away from the center towards the inner wall when the curvature ratio increases.

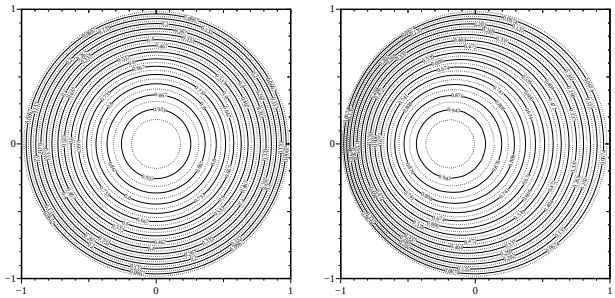

(a) $\delta = 0.001$ (b) $\delta = 0.5$

Figure 3: Axial velocity for creeping Newtonian flow.

As already known, for inertial Newtonian fluids ($\mathcal{R}e \neq 0$) a slight curvature of the pipe axis induces centrifugal forces on the fluid and consequently secondary flows, sending fluid outward along the symmetry axis and returning along the upper and lower curved surfaces. A pair of symmetric vortices is then superposed to the Poiseuille flow. This can be seen in Figure 4, where we contours of the axial velocity and the stream-function are presented for $\mathcal{R}e = 1$ and $\delta = 0.5$. The solutions obtained with FEM and Robertson's perturbation method show a good agreement, in accordance with the predictions. In particular, for this value of the curvature ratio, we can observe a shift from the center. The secondary flow is counter-clockwise in the upper half of the cross–section and clockwise in the lower half.

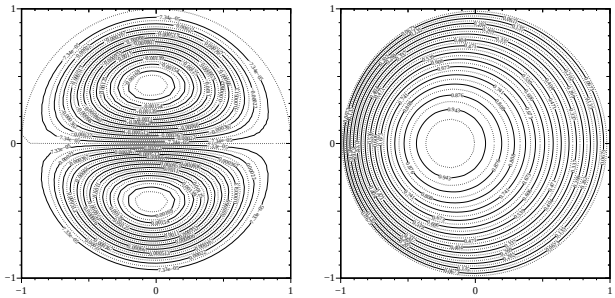

(a) (b)

Figure 4: Streamlines and axial velocity for Newtonian flows with $\mathcal{R}e = 1$ and $\delta = 0.5$.

4.2 Creeping viscoelastic flows

In this section, we are interested in the viscoelastic behaviour of the fluid in the case of creeping flows, and especially in the behaviour of the secondary motions.

Our numerical results (using the FEM) indicate changes in the flow characteristics and suggest that at zero Reynolds number, fluid viscoelasticity promotes a secondary flow. This phenomenon is also evident in the more general case of second-order fluids (with $\alpha_1 + \alpha_2 \neq 0$).

In Figure 5 and Figure 6, the streamlines are plotted for two distinct values of α_1. As in the case of the inertial Newtonian flow, the secondary flows involve non-zero values and are characterized by two counter-rotating vortices. However, their behaviour is not similar. In particular, the orientation of the contours of the stream function is opposite. As can be exepected, the magnitude of the secondary flows increase with the elastic level. Moreover, we observe that the flows remain symmetric relative to an axis which is identical to the pipe centerline for $|\alpha_1|$ small ($\alpha_1 = -10^{-2}$), and which slightly rotates counterclockwise when $|\alpha_1|$ increases ($\alpha_1 = -0.5$).

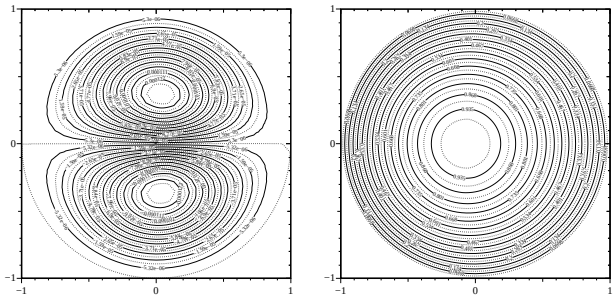

Figure 5: Streamlines and axial velocity for creeping viscoleastic flows with $\delta = 0.2$ and $\alpha_1 = -0.01$.

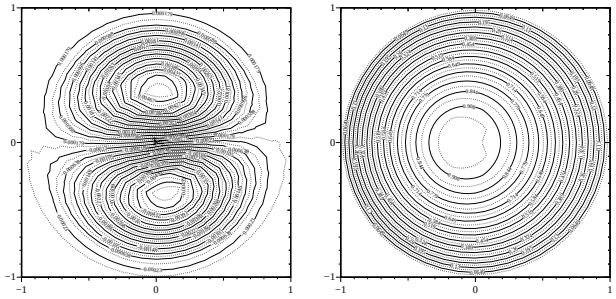

Figure 6: Streamlines and axial velocity for creeping viscoleastic flows with $\delta = 0.2$ and $\alpha_1 = -0.5$.

4.3 Inertial viscoelastic flows

Now, we are concerned with second-grade fluids where the Reynolds number $\mathcal{R}e$ is non-zero and set to 1.

We first consider a pipe with a small curvature ratio $\delta = 10^{-3}$. A comparison between our finite element solutions and Robertson's perturbation solutions shows a very satisfactory agreement for a small value of the viscoelastic constant α_1 ($\alpha_1 = -10^{-2}$). The secondary flows exist and have globally the same behaviour. At this stage, the nature and magnitude of the flow is qualitatively identical to that of a Newtonian fluid, the inertial effect being more pronouced and no effect due to viscoelasticity appears. The same behaviour can be observed for higher values of the curvature ratio.

When $|\alpha_1|$ increases, the solution obtained by FEM shows reversal flows whose nature is very close to that obtained in the case considered in the previous section when the secondary motion was generated by fluid viscoelasticity (see Figure 7).

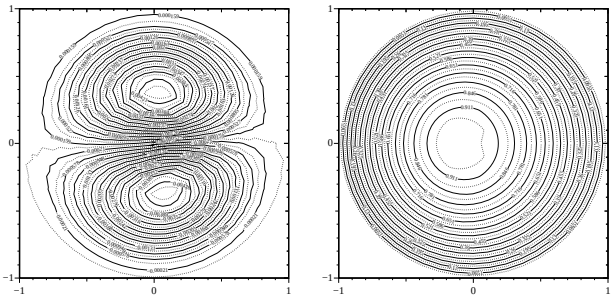

Figure 7: Streamlines and axial velocity for inertial viscoleastic flows with $\mathcal{R}e = 1$, $\delta = 0.2$, $\alpha_1 = -0.5$.

4.4 Effect of the viscoelasticity

Based on the remarks made in the previous sections, we now point out the influence of viscoelasticity in determining secondary flows. Our aim is to show that when the viscoelastic level increases, a transition from the Newtonian regime to a viscoelastic one occurs. The analysis was carried out for a Reynolds number set to one and the curvature ratio set to 0.5. Figure 8 presents the streamlines for different values of α_1 in the interval $[-0.01; -0.25]$. For $\alpha_1 = -0.01$ we are still in the Newtonian regime. Two counter-rotating vortices appear, and the streamlines in the core region are more dense than elsewhere. However, in Figure 8_b, a slight modification is already visible with the displacement of the vortices towards the inner wall. As α_1 increases, these facts become more pronounced.

The value $\alpha_1 = -0.05$ seems to be critical. The distortion of the streamlines is even more dramatic, and in addition to the vortices described below, another couple of vortices appear in the core region (see Figure 8_c). Interestingly, the values in this part of the cross-section have an opposite sign to the ones near the boundaries, suggesting that the core is the transition region and that the reversal from one state to another initiates there.

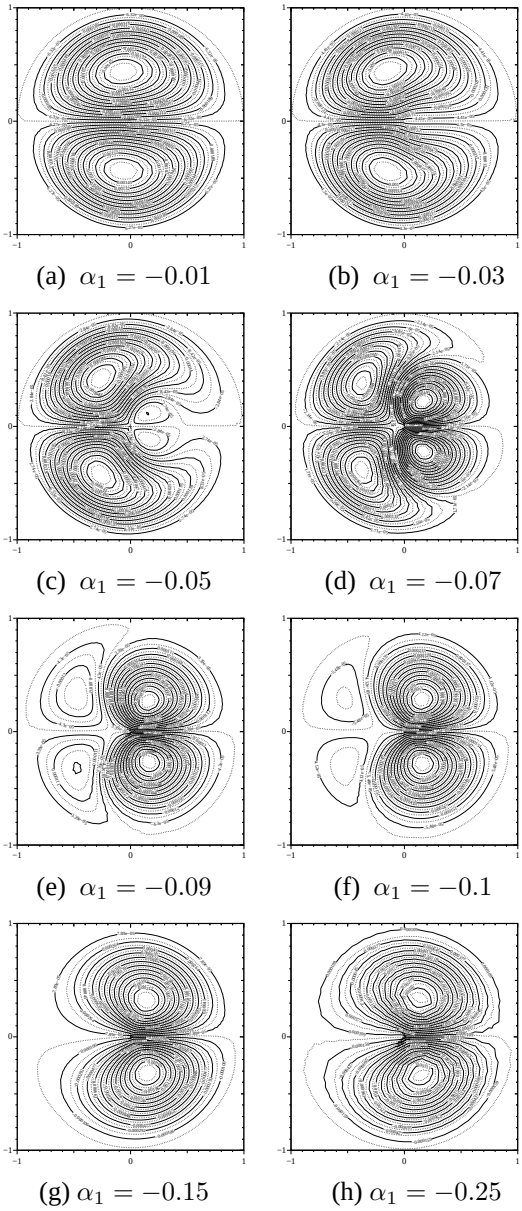

(a) $\alpha_1 = -0.01$ (b) $\alpha_1 = -0.03$

(c) $\alpha_1 = -0.05$ (d) $\alpha_1 = -0.07$

(e) $\alpha_1 = -0.09$ (f) $\alpha_1 = -0.1$

(g) $\alpha_1 = -0.15$ (h) $\alpha_1 = -0.25$

Figure 8: Effects of the viscoelasticity on the streamlines with $\mathcal{R}e = 1$ and $\delta = 0.5$.

This is confirmed by the results obtained for the cases where $\alpha_1 = -0.07, -0.09, -0.1$, showing that the reversal secondary flows grow around the new couple of vortices and that the changes occur from the core region to the regions near the boundary. It is clear that the size and strength of the new pair of vortices is more important, while a slackening of the streamlines and vortices corresponding to the Newtonian state is observed.

In Figure 8_g the transition from one regime to the other is completed. Finally, for $\alpha_1 = -0.25$ due to the combined effect of curvature and viscoelasticity, we observe a slight displacement of the center of the vortices to the outer wall.

4.5 Effect of the inertia

In the previous section, we observed that for fixed Reynolds number and curvature ratio, an increase of the viscoelastic parameter $|\alpha_1|$ induces a modification in the nature of the flow, passing from the Newtonian regime into the purely viscoelastic one. Our aim here is to consider the reversal phenomenon. Fixing the parameters α_1 and δ, we study the effect of fluid inertia.

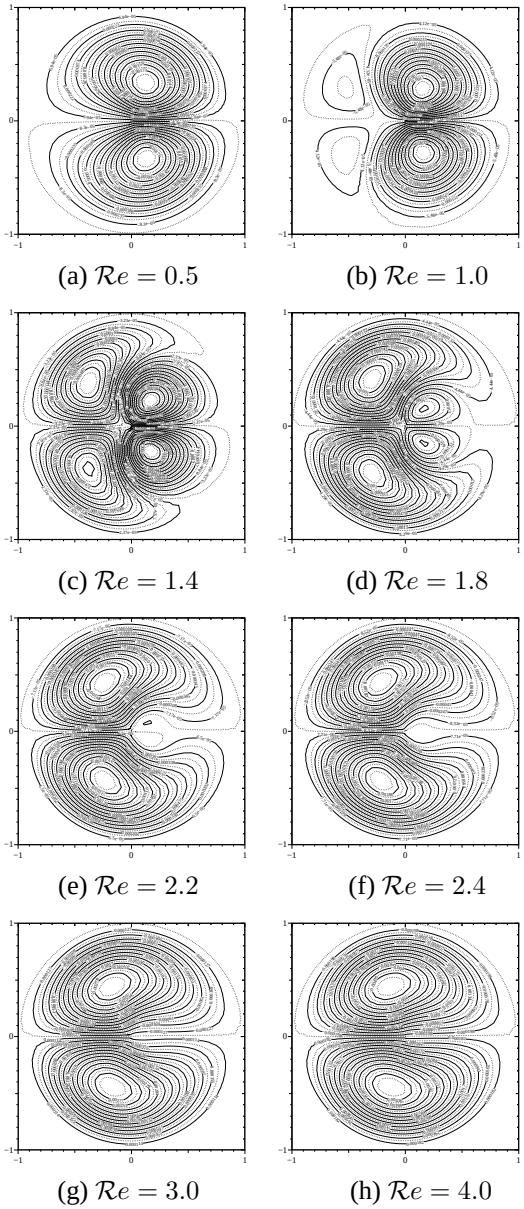

(a) $\mathcal{R}e = 0.5$ (b) $\mathcal{R}e = 1.0$

(c) $\mathcal{R}e = 1.4$ (d) $\mathcal{R}e = 1.8$

(e) $\mathcal{R}e = 2.2$ (f) $\mathcal{R}e = 2.4$

(g) $\mathcal{R}e = 3.0$ (h) $\mathcal{R}e = 4.0$

Figure 9: Effects of the inertia on the streamlines with $\alpha_1 = -0.1$ and $\delta = 0.5$.

Setting α_1=-0.1 and δ=0.5, we present in Figure 9 the contour plots of the stream function for different

values of $\mathcal{R}e$ in the interval $[0.5, 4]$.

For $\mathcal{R}e = 0.5$, the viscoelasticity is dominant and the inertial forces have no real effect on the secondary flows. For $\mathcal{R}e = 1$, some modifications occur. The streamlines in the core region appear to be less dense, the size of the couple of vortices is smaller, the flow is driven near the wall pipe. Moreover, we observe the formation of boundary layer flows, with a pair of weak and elongated vortices.

As Reynolds number increases, the boundary layer flows increase rapidly. The vortices in the core region are weaker, while the streamlines near the pipe wall are more dense and distorted, and a strenghthening of the new vortices becomes clear. There is evidence that in contrast with the case where the viscoelasticity dominates, the wall pipe here is the transition region from the viscoelastic state to the inertial one, and that the reversal flows, formed near the boundary around the new vortices, develop and drive the flow to the center of the pipe.

5 Conclusion

This paper is devoted to finite element simulations of steady fully developed flows of second-grade fluids in curved pipes of circular cross section and arbitrary curvature ratio, driven by a pressure drop. The qualitative behaviour of the secondary flows with respect to the different parameters of the problem was analyzed to study the corresponding inertial and viscoelastic effects. The numerical results have been validated through the comparison with those obtained by using a perturbation method [10]. Details can be found in [5]. A more complete discussion will the object of a forthcoming work.

Acknowledgements: This work has been partially supported by the grant SFRH/BPD/3506/2000 of Fundação para a Ciência e a Tecnologia (N. Arada), Fundação Calouste Gulbenkian (P. Correia), Center for Mathematics and its Applications (CEMAT) through FCT's Funding Program, and through the Projects POCTI/MAT/380/2001 and POCTI/MAT/41898/2001.

References:

[1] N. Arada, P. Correia and A. Sequeira, Analysis and finite element simulations of a second-order fluid model in a bounded domain, submitted.

[2] N. Arada, M. Pires and A. Sequeira, Viscosity effects on flows of generalized Newtonian fluids through curved pipes, *Computers and Mathematics with Applications*, 2005, accepted for publication.

[3] N. Arada, M. Pires and A. Sequeira, Numerical simulations of shear-thinning Oldroyd-B fluids in curved pipes, *IASME Transactions*, Issue 6, 2, 2005, pp. 948-959.

[4] R. B. Bird, R. C. Armstrong and O. Hassager, *Dynamics of polymeric liquids*, John Wiley & Sons, New York (1987).

[5] P. Correia, *Numerical simulations of a non–Newtonian fluid flow model using finite element methods*, PhD Thesis, IST/UTL, 2004.

[6] V. Coscia and A. Robertson, Existence and uniqueness of steady, fully developed flows of second order fluids in curved pipes, *Math. Models Methods Appl. Sci.* 11, 2001, pp. 1055–1071.

[7] W.R. Dean, Note on the motion of fluid in curved pipe, *Philos. Mag.* 4, 1927, pp. 208–223.

[8] W.R. Dean, The streamline motion of fluid in curved pipe, *Philos. Mag.* 5, 1928, pp. 673–695.

[9] Y. Fan, R. I. Tanner and N. Phan-Thien, Fully developed viscous and viscoelastic flows in curved pipes, *J. Fluid Mech.*, 440, 2001, pp. 327-357.

[10] W. Jitchote and A.M. Robertson, Flow of second order fluids in curved pipes, *J. Non–Newtonian Fluid Mech.* 90, 2000, pp. 91–116.

[11] A. M. Robertson, On viscous flow in curved pipes of non-uniform cross section, *Inter. J. Numer. Meth. fluid.* 22, 1996, pp. 771–798.

[12] W.Y. Soh and S.A. Berger, Fully developed flow in a curved pipe of arbitrary curvature ratio, *Int. J. Numer. Meth. Fluid.* 7, 1987, pp. 733–755.